Magneto-Structural Correlation in Two Isomeric Series of Nitronyl Nitroxide Molecular Magnets: Intermolecular Interactions Relevant to Ferromagnetic Exchange in Naphthyl and Quinolyl Derivatives

T. Sugano,*,† M. Kurmoo,†,[1] H. Uekusa,‡ Y. Ohashi,‡ and P. Day†

*Department of Chemistry, Meiji Gakuin University, Kamikurata, Totsuka-ku, Yokohama 244, Japan; †The Davy Faraday Research Laboratory,
The Royal Institution of Great Britain, 21 Albemarle Street, London W1X 4BS, United Kingdom; and ‡Department of Chemistry, Faculty of Science,
Tokyo Institute of Technology, Ookayama, Meguro-ku, Tokyo 152, Japan

Two isomeric series of stable organic free radicals, 1- and 2-naphthyl nitronyl nitroxide (1- and 2-NAPNN) and 2-, 3-, and 4-quinolyl nitronyl nitroxide (2-, 3-, and 4-QNNN), were synthesized and their crystal structures were determined by X-ray diffraction. The crystal structure of 1-NAPNN consists of a three-dimensional (3D) molecular network formed by several atomic contacts between the O atom of the ONCNO group and the aromatic ring as well as between the O atom and the methyl groups. Since 1-NAPNN shows intra- and interlayer ferromagnetic (FM) intermolecular interactions with exchange coupling constants $J/k = 0.09$ K and $J'/k = 0.03$ K ($\mathcal{H} = -2J\sum S_i S_j$), respectively, these contacts are relevant to the FM intermolecular interaction. In contrast, 4-QNNN, having a molecular structure close to that of 1-NAPNN, contains molecular chains with alternating antiferromagnetic (AFM) intermolecular interaction with $J/k = -7.8$ K and $\alpha = 0.5$ [$\mathcal{H} = -2J\sum (S_{2i-1}S_{2i} + \alpha S_{2i}S_{2i+1})$]. The crystal structures of 2-NAPNN, 2-QNNN, and 3-QNNN consist of 2D molecular layers formed through contacts similar to those observed in 1-NAPNN. The radical molecules are oriented in the same direction forming a herringbone-like arrangement in the layers. 2-NAPNN exhibits interlayer AFM interaction with $J'/k = -0.31$ K in addition to FM interaction with $J/k = 0.14$ K in the layer, whereas 2- and 3-QNNN show 3D FM intermolecular interactions with $J/k = 0.018$ K, $J'/k = 0.01$ K (2-QNNN) and $J/k = 0.12$ K, $J'/k = 0.03$ K (3-QNNN). Each layer in 2-NAPNN is related to adjacent layers by twofold screw symmetry to yield atomic contacts between the naphthyl rings standing opposite across the interface of the layers. Since the contacts between the aromatic rings of these nitronyl nitroxides favor AFM intermolecular interaction while the contacts within the 2D layer favor FM interaction, 2-NAPNN shows overall AFM behavior. In contrast, the crystals of 2- and 3-QNNN have no such twofold axis and hence the 2D FM layers are connected through interlayer contacts, which result overall in FM behavior. Possible origins of the characteristic molecular arrangements that give rise to FM intermolecular interaction in the 2D layer are discussed in terms of hydrogen-bond formation between the O atom of the ONCNO group and the methyl groups of the nitronyl nitroxide moieties. © 1999 Academic Press

INTRODUCTION

Organic molecular magnetism (1) has developed rapidly since the first discovery of a purely organic ferromagnet (2). A rich variety of magnetic behavior, such as ferro-, anti-ferro-, weak ferro- (canted), and meta-magnetism, has been observed in molecular crystals containing organic radicals as spin centers. Bulk ferromagnetism has been reported for the nitronyl nitroxide (2-imidazoline-1-oxyl 3-oxide) (2–5), nitroxide (aminoxyl) (6–9), and verdazyl (10–11) radicals, while weak ferromagnetism is observed in several organic ion radical salts with nonmagnetic inorganic counter ions (12–13) and even for purely organic materials (14–20). Meta-magnetic behavior is reported for the nitroxide monoradical (21) and diradical (22).

These developments have given considerable insight into organic magnetism, but the detailed mechanism of the ferromagnetic (FM) intermolecular interactions in organic materials still remains open to question. To gain a more precise understanding of the mechanism, one approach is to correlate the magnetism with the molecular packing in crystals composed of radicals with a very similar molecular structure. Such a program can only be carried out on materials with sufficient chemical stability and crystallinity. The nitronyl nitroxide radical is known to be stable even in a solution and it can be purified by column chromatography (23). So conventional methods can be used to grow single crystals of nitronyl nitroxide-containing derivatives. Furthermore, they often exhibit ferromagnetic intermolecular interactions (1).

Since numerous derivatives can be synthesized (23), we have been investigating magnetic properties and crystal structures of the aromatic (hetero)cyclic derivatives of nitronyl nitroxide, especially polycyclic derivatives (24–28). The aim of using polycyclic aromatic substituents is twofold. First, extending the conjugated π system should favor FM intermolecular interaction, because it reduces the energy separation between the two frontier orbitals (the singly occupied molecular orbital (SOMO) and the next-highest doubly occupied molecular orbital (NHOMO)), increasing the already considerable spin-polarization effect characteristic of nitronyl nitroxide (29, 30). Second, extending the size of the substituent moiety favors higher dimensional magnetic interactions through interatomic contacts among neighboring molecules. Higher dimensionality of magnetic interaction is of primary importance in establishing bulk magnetic order in the solid.

We have shown that 3-quinolyl nitronyl nitroxide [2-(3-quinolyl)-4,4,5,5-tetramethyl-2-imidazoline-1-oxyl 3-oxide, abbreviated as 3-QNNN] exhibits FM intermolecular interaction (26) and a phase transition to a magnetically ordered state below 0.21 K (14, 19, 20), and that 1-naphthyl nitronyl nitroxide [2-(1-naphthyl)-4,4,5,5-tetramethyl-2-imidazoline-1-oxyl 3-oxide, abbreviated as 1-NAPNN], whose chemical formula is very close to 3-QNNN (a =CH– group of the naphthyl ring of NAPNN is replaced by a N atom in QNNN as seen in Fig. 1a), exhibits FM intermolecular interaction (20) and a phase transition to a magnetically ordered state below 0.10 K (31). On the other hand, 4-quinolyl nitronyl nitroxide (4-QNNN) and 2-naphthyl nitronyl nitroxide (2-NAPNN), which are structural isomers of 1-NAPNN and 3-QNNN, respectively, exhibit antiferromagnetic (AFM) behavior (20, 27). These remarkable differences in the intermolecular magnetic interactions among the isomers of NAPNN and QNNN suggest that a closer examination of the magnetic and crystallographic properties of the two series, 1- and 2-NAPNN and 2-, 3-, and 4-QNNN, may afford useful insight into magnetostructural correlations in organic radical solid.

In this paper we first describe the crystal structures of 1- and 2-NAPNN, and 2-, 3-, and 4-QNNN with emphasis on the intermolecular contacts among the aromatic ring and the NO and methyl groups of the nitronyl nitroxide moiety. We show that the almost identical molecular structures of 2-NAPNN, 2-QNNN, and 3-QNNN give rise to a common two-dimensional (2D) arrangement of molecules in their crystals, although the interlayer molecular packing that yields a three-dimensional (3D) network in 2-NAPNN is quite different from that of 2- and 3-QNNN. Next, the magnetic properties of the crystals are described: 1-NAPNN, 2-QNNN, and 3-QNNN show FM intermolecular interaction, whereas 2-NAPNN and 4-QNNN exhibit AFM interaction. Finally, it is possible to relate the 2D molecular arrangement to the FM intermolecular

interaction in these nitronyl nitroxide radicals. In addition, the molecular arrangements of 1-NAPNN and 4-QNNN, whose molecular structures are very similar to each other, are compared with those of 2-NAPNN, 2-QNNN, and 3-QNNN in terms of weak hydrogen-bond formation linking the O atoms of the NO groups or N atom on the quinolyl ring to the H atoms of the methyl groups.

EXPERIMENTAL

The two isomeric series of naphthyl and quinolyl nitronyl nitroxides were synthesized by the reaction of the corresponding naphthalenecarbaldehyde and quinolinecarbaldehyde, which were purchased from Aldrich Chemical Co. Ltd. with 2,3-bis(hydroxylamino)-2,3-dimethylbutane (32) in methanol, by following the oxidation with lead(IV) dioxide in benzene according to the procedures reported (23): typical yield; 1-NAPNN, 52%; 2-NAPNN, 30%; 2-QNNN, 58%; 3-QNNN, 60%; 4-QNNN, 62%. Crystals suitable for X-ray diffraction studies were grown by slow cooling or slow evaporation in the dark of concentrated solutions of 1- and 2-NAPNN in methanol and 2-, 3-, and 4-QNNN in benzene. No solvent inclusion into the crystals was observed.

X-ray diffraction intensities were recorded on a Rigaku AFC5R automatic four-circle diffractometer with graphite monochromatized Mo$K\alpha$ ($\lambda = 0.71069$ Å) radiation at room temperature (296 K). Unit-cell dimensions were obtained by a least-squares refinement for $19 \sim 25$ reflections with $20° < 2\theta < 25°$ except for 2-QNNN. For 2-QNNN, unit cell dimensions were determined for 19 reflections with $10° < 2\theta < 14°$ because of weak reflections at higher angles. During data collection, the intensities of 3 representative reflections were examined every 50 reflection measurements and no crystal deterioration was observed. Intensity data were corrected for Lorentz and polarization effects but not for absorption. The crystal structure was solved by direct methods and the positions of H atoms were calculated. A full-matrix least-squares refinement was carried out, in which positions of the non-H atoms were treated with anisotropic thermal parameters and those of H atoms were treated with isotropic parameters. The difference Fourier synthesis after the refinement showed no peak with an intensity stronger than 0.35 e Å^{-3}. Crystallographic data are listed in Table 1. Final positional parameters and equivalent isotropic thermal parameters for 1- and 2-QNNN and 2- and 4-QNNN are given in Tables S1–S4, respectively, as deposited material to NAPS (see Footnote 1). These parameters for 3-QNNN were described in (26).

Magnetization isotherms up to 7 T and static magnetic susceptibility from 1.8 to 300 K were measured with a Quantum Design MPMS7 SQUID magnetometer using polycrystalline samples held in a gelatin capsule inside a plastic tube. The susceptibility below 30 K was measured
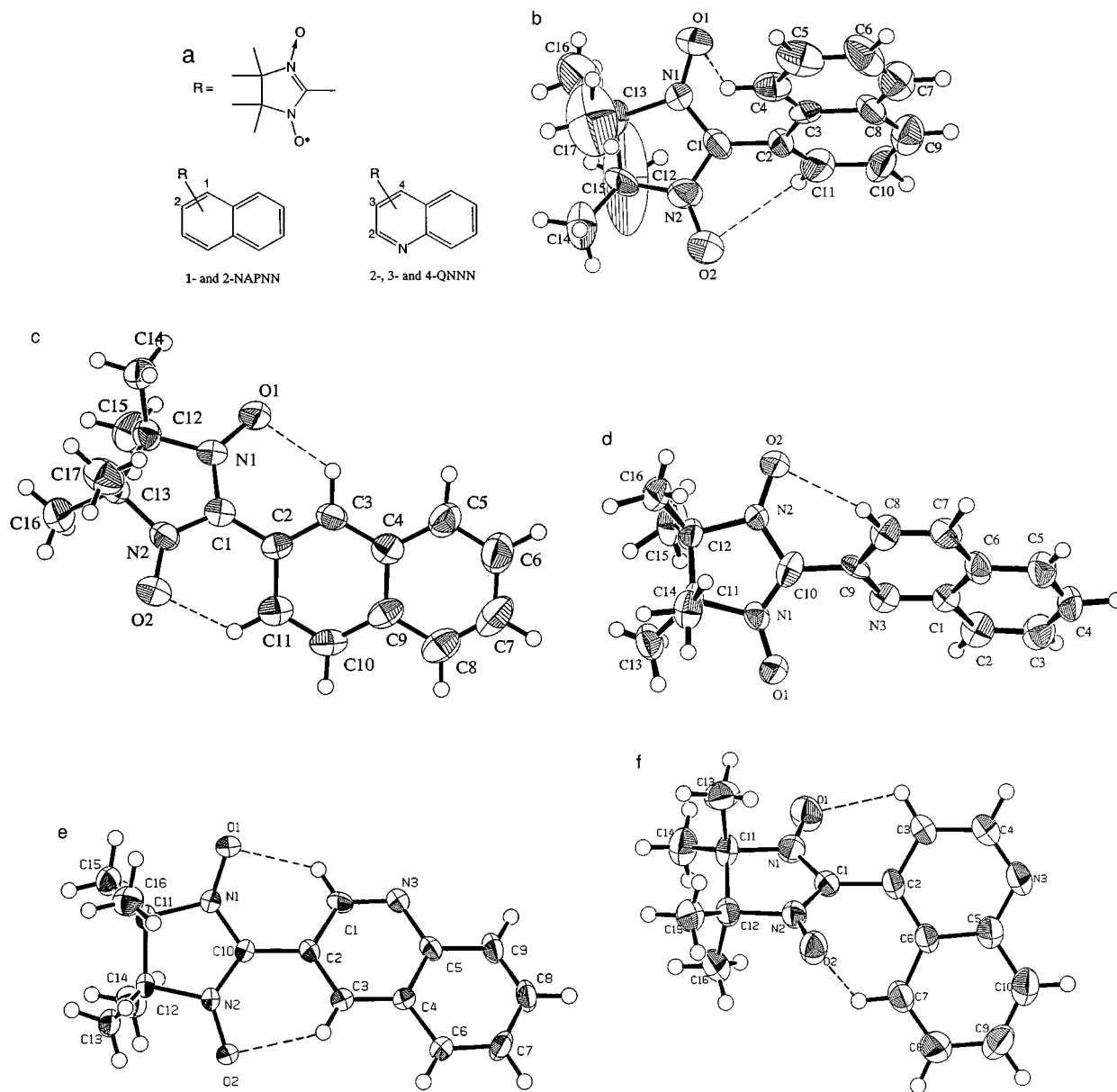
FIG. 1. (a) Structural formulas of the isomers of naphthyl nitronyl nitroxide (NAPNN) and quinolyl nitronyl nitroxide (QNNN). ORTEP (33) drawings of the molecular geometries of (b) 1-NAPNN, (c) 2-NAPNN, (d) 2-QNNN, (e) 3-QNNN, and (f) 4-QNNN showing the atomic numbering schemes. The dashed lines represent intramolecular hydrogen–oxygen contacts.

at 0.1 T to avoid saturation effects. The diamagnetic contribution was estimated from the data above 200 K by assuming that paramagnetic susceptibilities follow the Curie–Weiss law.

RESULTS AND DISCUSSION

3.1. Molecular and Crystal Structures

Only one molecule is crystallographically independent in all the crystals of 1- and 2-NAPNN and 2-, 3-, and 4-QNNN. The molecular geometry of each radical is shown in Figs. 1b–1f with the atomic numbering scheme. Selected bond lengths and angles of the five-membered nitronyl nitroxide moieties are given in Table 2. They compare well to those reported for other 2-substituted (α-) nitronyl nitroxides. Both the O–N–C–N–O group and the dicyclic aromatic group of each radical are planar with maximum deviations of 0.039 and 0.047 Å, respectively. The dihedral angles between the planes of the ONCNO group and the dicyclic group of 1-NAPNN (60.9°), 2-QNNN (54.5°), and

<div align="center">

TABLE 1
Crystallographic Data for 1- and 2-NAPNN and 2-, 3-, and 4-QNNN

</div>

	1-NAPNN	2-NAPNN	2-QNNN	3-QNNN[a]	4-QNNN
Empirical formula	$C_{17}H_{19}N_2O_2$	$C_{17}H_{19}N_2O_2$	$C_{16}H_{18}N_3O_2$	$C_{16}H_{18}N_3O_2$	$C_{16}H_{18}N_3O_2$
Formula weight	283.35	283.35	284.34	284.34	284.34
Crystal color, habit	black, plate	black, needle	black, plate	black, block	black, plate
Crystal dimensions (mm)	$0.4 \times 0.2 \times 0.1$	$0.4 \times 0.3 \times 0.1$	$0.5 \times 0.4 \times 0.2$	$0.5 \times 0.3 \times 0.3$	$0.5 \times 0.3 \times 0.2$
Crystal system	monoclinic	orthorhombic	monoclinic	monoclinic	triclinic
Space group	Cc (No. 9)	$P2_12_12_1$ (No. 19)	Cc (No. 9)	$P2_1$ (No. 4)	$P\bar{1}$ (No. 2)
Lattice parameters					
a (Å)	12.492(4)	11.087(4)	6.575(4)	10.5356(8)	10.44(1)
b (Å)	7.676(4)	22.020(4)	20.332(5)	11.0273(7)	10.678(7)
c (Å)	15.925(3)	6.156(4)	11.409(5)	6.1267(5)	7.302(3)
α (deg)					102.29(4)
β (deg)	96.91(2)		94.23(4)	94.255(6)	102.41(7)
γ (deg)					68.55(8)
V (Å^3)	1515.8(8)	1503(1)	1520(1)	709.83(8)	732(1)
Z value	4	4	4	2	2
D_{calc} (g cm^{-3})	1.24	1.25	1.24	1.33	1.29
Radiation	Mo$K\alpha$	Mo$K\alpha$	Mo$K\alpha$	Cu$K\alpha$	Mo$K\alpha$
μ (cm^{-1})	0.82	0.83	0.84	6.88	0.81
Number collected	1959	2018	2198	2608	2813
Number observed	733	935	974	1154	1222
	($I > 1.5\sigma(I)$)	($I > 1.5\sigma(I)$)	($I > 2.0\sigma(I)$)	($I > 3.0\sigma(I)$)	($I > 3.0\sigma(I)$)
R	0.088	0.064	0.076	0.062	0.072
R_w	0.062	0.046	0.078	0.082	0.075

[a] Ref. 26.

4-QNNN (51.7°) are over twice as large as those of 2-NAPNN (26.7°) and 3-QNNN (24.8°).

In 1-NAPNN and 4-QNNN, steric repulsion between one of the NO groups and a H atom of the second six-membered ring of the dicyclic group results in large dihedral angles, as shown in Figs. 1b and 1f. The O $\cdots$ H distances are 2.82(1) (O1 $\cdots$ H) and 2.90(1) Å (O2 $\cdots$ H) for 1-NAPNN and 2.73(1) (O1 $\cdots$ H) and 2.53(1) Å (O2 $\cdots$ H) for 4-QNNN. These distances are longer than the sum of the van der Waals radii (34) of hydrogen (1.2 Å) and oxygen (1.4 Å) except for one of the distances of 4-QNNN, thereby indicating no intramolecular hydrogen bond.
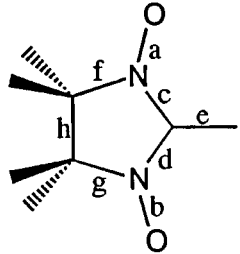
In contrast, steric repulsion is avoided in 2-NAPNN and 3-QNNN because the second six-membered ring is geometrically far from the nitronyl nitroxide group, as shown in Figs. 1c and 1e. This reduction in the steric repulsion allows H $\cdots$ O contacts between the ONCNO and dicyclic groups. As a result, in 2-NAPNN and 3-QNNN, intramolecular hydrogen-bonds are formed between the two N-bonded O atoms and the two H atoms of the first six-membered ring. The O $\cdots$ H distances are 2.28(1) (O1 $\cdots$ H) and 2.42(1) Å (O2 $\cdots$ H) for 2-NAPNN and 2.30(1) (O1 $\cdots$ H) and 2.31(1) Å (O2 $\cdots$ H) for 3-QNNN. These distances are shorter than the sum of the van der Waals radii (2.6 Å), suggesting weak hydrogen bonds between the O and H atoms. These intramolecular hydrogen bonds are responsible for the small dihedral angles seen in 2-NAPNN and 3-QNNN.

In 2-QNNN, whose molecular shape is close to those of 2-NAPNN and 3-QNNN, however, only one H $\cdots$ O contact is possible because there is no H but N atom on the other side of the first ring, as shown in Fig. 1d. Consequently, the O $\cdots$ H distance is elongated to 2.71(1) Å, which is longer than the sum of the van der Waals radii. Therefore, there is no intramolecular hydrogen bond to reduce the dihedral angle, with the consequence that the dihedral angle in 2-QNNN is twice as large as in 2-NAPNN and 3-QNNN.
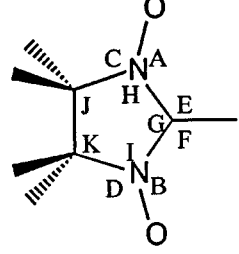
In describing the crystal structures of 1- and 2-NAPNN and 3- and 4-QNNN, we concentrate on the relative orientations of molecules. As we shall show below, there are three kinds of interatomic contacts between neighboring molecules that are relevant to magnetic interaction. For clarity, the contacts between the O atoms of the ONCNO group and the aromatic dicyclic ring, those between the O atoms and the methyl groups, and those between the ONCNO groups and between the dicyclic rings themselves are represented by solid lines, dashed lines, and dotted lines, respectively, in the figures.

1-NAPNN crystallizes in the monoclinic system with space group Cc and $Z = 4$. The crystal structure projected along the a axis is shown in Fig. 2a. The 1-NAPNN molecules are oriented in the same direction along the c axis. There are several intermolecular contacts between the O atoms of the ONCNO group and the naphthyl ring as well as

TABLE 2
Selected Bond Distances (Å) and Angles (°) of Nitronyl Nitroxide Moieties of the Isomers of NAPNN and QNNN

Bond distances   Bond angles

		1-NAPNN	2-NAPNN	2-QNNN	3-QNNN	4-QNNN
			Bond distances			
N–O	a	1.27(1)	1.289(5)	1.26(1)	1.281(8)	1.271(6)
	b	1.30(1)	1.289(6)	1.27(1)	1.292(8)	1.265(6)
N–C	c	1.36(1)	1.347(7)	1.39(1)	1.334(9)	1.333(7)
	d	1.34(1)	1.362(7)	1.29(1)	1.36(1)	1.333(7)
C–C	e	1.44(2)	1.457(8)	1.47(1)	1.46(1)	1.491(7)
N–C	f	1.52(1)	1.495(7)	1.53(1)	1.51(1)	1.514(7)
	g	1.51(1)	1.499(7)	1.51(1)	1.505(9)	1.526(7)
C–C	h	1.47(2)	1.558(8)	1.54(2)	1.55(1)	1.553(8)
			Bond angles			
	A	124.6(8)	125.3(5)	127.9(9)	126.8(6)	128.0(5)
	B	125(1)	126.0(5)	126.7(9)	126.8(6)	128.6(5)
	C	124(1)	120.8(4)	122.6(8)	120.0(5)	121.7(5)
	D	121.1(9)	120.5(5)	121.3(8)	121.1(6)	121.2(5)
	E	128.9(9)	126.2(6)	121(1)	125.6(7)	124.7(5)
	F	124(1)	126.1(6)	128(1)	125.3(7)	124.0(5)
	G	106.8(9)	107.7(5)	111.3(9)	109.0(6)	111.1(5)
	H	111.3(9)	113.3(5)	108.9(9)	112.8(6)	110.0(4)
	I	112.8(9)	113.0(5)	110.8(9)	111.8(6)	109.9(4)
	J	103(1)	101.3(5)	100.2(8)	100.9(6)	99.8(4)
	K	102(1)	101.1(5)	102.4(8)	101.8(6)	100.0(4)

between the O atoms and methyl groups of neighboring molecules. The interatomic distances relevant to the intermolecular contacts are summarized in Table 3. The O1(i′)–C7(i) contact is along the b axis and the O2(i)–C7(ii), O2(i)–C9(ii), and O1(ii′)–C14(i) contacts are along the c axis as shown by the solid and dashed lines in Fig. 2a. These contacts therefore form 2D molecular layers parallel to the bc plane. The 2D molecular layer may be regarded as a distorted square lattice since the bc plane is face centered.

The 2D molecular layers are connected along the [110] direction in the (001) plane and along the [$\bar{1}$10] direction in the (002) plane by intermolecular contacts as shown by the solid and dashed lines in Fig. 2b. Of these contacts, the O2(iii)–C17(i) and O2(iv)–C17(ii′) distances are 3.34(2) Å, shorter than the sum of the van der Waals radii of O atom and methyl group (3.4 Å), thereby suggesting intermolecular hydrogen bonds between the O atoms of the ONCNO

group and H atoms of the methyl groups. The contacts between the layers, together with the contacts within the 2D layers, yield a 3D molecular network in 1-NAPNN.

2-NAPNN crystallizes in the orthorhombic system with space group $P2_12_12_1$ and $Z = 4$. The crystal structure projected along the c and a axes is shown in Fig. 3. The molecular arrangement of 2-NAPNN in the half of the unit cell divided at the (020) plane (of which a side view is shown by the dash-dotted line in Fig. 3) is quite similar to that found in 3-QNNN (see below), which shows FM intermolecular interaction (26) and has a molecular structure close to 2-NAPNN. In the half of the unit cell, the 2-NAPNN molecules are oriented in the same direction along the a axis, while the screw symmetry of molecular arrangement along the a axis moves the neighboring 2-NAPNN molecules apart to form a herringbone-like structure.

There are several intermolecular contacts between the O atoms of the ONCNO group and the methyl groups of neighboring molecules. The relevant interatomic distances are listed in Table 4. Of these contacts, the distance for the contact O1(i)–C14(iii′), 3.256(8) Å, is shorter than the sum of the van der Waals radii of O atom and methyl group (3.4 Å), indicating intermolecular hydrogen bonds as observed in 1-NAPNN. Since the contacts between the molecules i and iii′ are along the a axis and the contacts between i and i′ as well as iii and iii′ are along the c axis, these intermolecular contacts between the NO and methyl groups form 2D molecular layers parallel to the ac plane. Although the 2D layer is not flat but corrugated, it may be regarded as a square lattice.

The molecular orientations in the other half of the unit cell are reversed as a result of the twofold screw symmetry along the b axis. Consequently, there are several intermolecular contacts between the naphthyl rings standing opposing one another across the (020) plane, as represented by the dotted lines in Fig. 3. The distances of these contacts are also listed in Table 4. The interatomic contacts between the dicyclic (naphthyl in 2-NAPNN) rings of molecules, which are laid on the neighboring 2D layers one by one, are not observed in 2- and 3-QNNN having molecular structures similar to 2-NAPNN, as described below.

2-QNNN crystallizes in the monoclinic system with space group Cc and $Z = 4$. The crystal structure projected along the a and c axes is shown in Fig. 4. Although the space group is the same as that of 1-NAPNN, the arrangement of the 2-QNNN molecules is quite different from that of 1-NAPNN except that they are all oriented in the same direction along the c axis due to the symmetry requirement of the space group. The disposition of the molecules in the 2-QNNN crystal is quite similar to that in 2-NAPNN and 3-QNNN, whose molecular structures are very close to that of 2-QNNN. More strictly speaking, however, the geometrical relations among the neighboring molecules in 2-QNNN differ from those in 2-NAPNN and 3-QNNN, because the
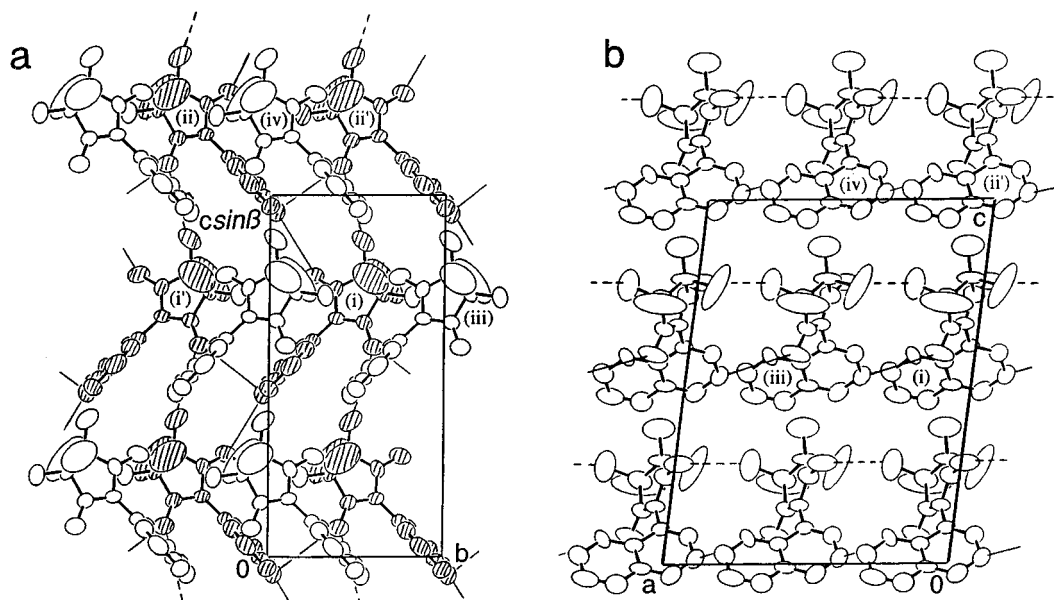
FIG. 2. Crystal structure of 1-NAPNN: (a) relation between two 2D layers projected along the *a* axis; shaded molecules are on the lower layer; (b) projection along the *b* axis (side view of the layers). Note that all the molecules are oriented in the same direction along the *c* axis. Solid and dashed lines represent the intermolecular contacts relevant to magnetic interaction. For the symmetry operations, see Table 3.

crystal of 2-QNNN has no screw axis but a glide plane while those of 2-NAPNN and 3-QNNN have twofold screw axes.

There are interatomic contacts between the O atoms of the ONCNO group and methyl groups as well as between the O atom and the quinolyl ring, as shown by the dashed lines in Fig. 4. The relevant distances are given in Table 5. The O1(i)–C16(ii′) distance is 3.37 Å and comparable to the sum of the van der Waals radii of O atom and methyl group (3.4 Å). Since the contacts between the molecules i and ii′ are along the *c* axis while the contacts between i and i′ are along the *a* axis, these intermolecular contacts form 2D molecular layers parallel to the *ac* plane. The 2D layer may be regarded as a square lattice, although it is not flat but corrugated, as mentioned for 2-NAPNN.

The 2D molecular layers are connected along the [$\bar{1}$01] direction by the contacts between the O atoms of the NO

group of molecule i′ and the naphthyl ring of molecule iv. No intermolecular contacts between the dicyclic (quinolyl) rings are observed. The contacts shown by the solid lines in Fig. 4b thus constitute a 3D network of the molecules. The lack of a screw axis in 2-QNNN, which relates the 2D molecular layers of 2-NAPNN in a different way, results in a remarkable difference between the 3D arrangement of the molecules in these two crystals.

Although the crystal structure of 3-QNNN has already been published (26), we describe it here in more detail in order to compare it with the other compounds in the series. 3-QNNN crystallizes in the monoclinic system with space group $P2_1$ and $Z = 2$. The crystal structure projected along the *b* and *c* axes is shown in Fig. 5. There are intermolecular contacts between the O atoms of the ONCNO group and the methyl groups. The relevant interatomic distances are summarised in Table 6. The O2(i)–C13(ii) distance 3.28(1) Å is shorter, and the distance 3.44(2) Å for the contact O2(i)–C15(ii) is close to the sum of the van der Waals radii of O and methyl group, thereby indicating intermolecular hydrogen bonds. Since the contacts between the molecules i and ii are along the *b* axis and the contact between i and i′ is along the *c* axis, the intermolecular contacts result in 2D layers parallel to the *bc* plane. The layer may be regarded as a square lattice as in 2-NAPNN. It is worth noting that the contacts O2–C13, O2–C15, and O1–C16 in 3-QNNN correspond, respectively, to O1–C14, O1–C16, and O2–C17 in 2-NAPNN, because both radical crystals have screw axes, respectively, along the *b* axis in 3-QNNN and along *a* in 2-NAPNN. The correspondence

TABLE 3
Intermolecular Distances of 1-NAPNN[a]

Intralayer contact	$r/Å$	Interlayer contact	$r/Å$
O1(i′)–C7(i)	3.55(2)	O1(i)–C10(iii)	3.54(2)
O2(i)–C7(ii)	3.57(2)	C17(i)–O2(iii)	3.34(2)
O2(i)–C9(ii)	3.68(2)	O1(ii′)–C10(iv)	3.54(2)
O1(ii′)–C14(i)	3.41(2)	C17(ii)–O2(iv)	3.34(2)

[a] Symmetry operations: (i) x, y, z, (i′) $x, -1 + y, z$, (ii) $x, -y, 1/2 + z$, (ii′) $x, 1 - y, 1/2 + z$, (iii) $1/2 + x, 1/2 + y, z$, (iv) $1/2 + x, 1/2 - y, 1/2 + z$.
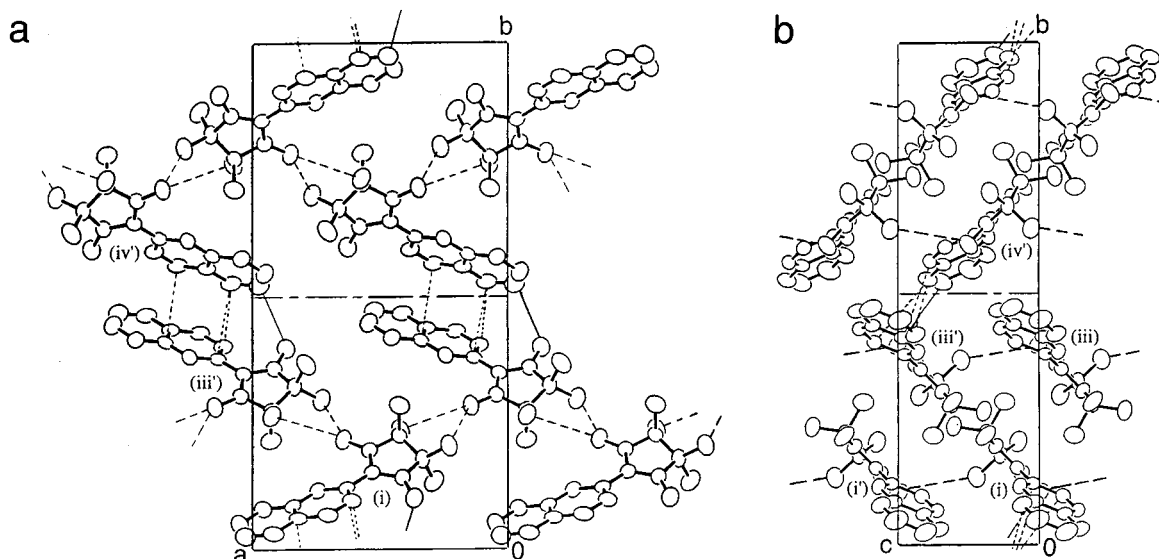
FIG. 3. Crystal structure of 2-NAPNN: (a) a side view of 2D layers projected along the c axis; (b) another side view of 2D layers projected along the b axis. Dash–dotted line indicates the side view of the (020) plane that partitions the unit cell into two subcells. Note that the molecules in the one half of the unit cell (i.e., subcell) are oriented in the same direction, whereas the molecular direction in the other subcell is reversed. Dashed lines represent the intermolecular contacts within the 2D layer and dotted and solid lines indicate interlayer intermolecular contacts. For the symmetry operations, see Table 4.

between these atomic contacts is especially interesting when comparing magnetic interactions in the two crystals.

The intermolecular contacts between layers are significantly different in 3-QNNN from those found in 2-NAPNN, in spite of the close similarity between the molecular arrangements within the 2D layers. Adjacent layers in 3-QNNN are related not by screw symmetry but transverse symmetry along the b axis, because the unit-cell volume (709.83(8) Å^3) as well as the lattice constant of the b axis (11.0273(7) Å) of 3-QNNN are half as small as those of 2-NAPNN (1503(1) Å^3 and 22.020(4) Å) due to the lack of the screw symmetry along the b axis in 3-QNNN. Consequently, all the molecules in the 3-QNNN crystal are oriented in the same direction, whereas, in 2-NAPNN, the molecules in one half of the unit cell divided at the middle

TABLE 4
Intermolecular Distances of 2-NAPNN[a]

Intralayer contact	r/Å	Interlayer contact	r/Å
O1(i)–C14(iii′)	3.256(8)	C2(iii′)–C8(iv′)	3.540(8)
O1(i)–C16(iii′)	3.514(8)	C4(iii′)–C10(iv′)	3.623(8)
O2(i′)–C17(i)	3.586(8)	C11(iii′)–C8(iv′)	3.653(9)
		O2(iii′)–C7(iv′)	3.563(9)

[a] Symmetry operations: (i) x, y, z, (i′) $x, y, 1 + z$, (ii) $1/2 - x, -y, 1/2 + z$, (iii) $1/2 + x, 1/2 - y, z$, (iii′) $1/2 + x, 1/2 - y, 1 + z$, (iv′) $2 - x, 1/2 + y, 1/2 - z$.
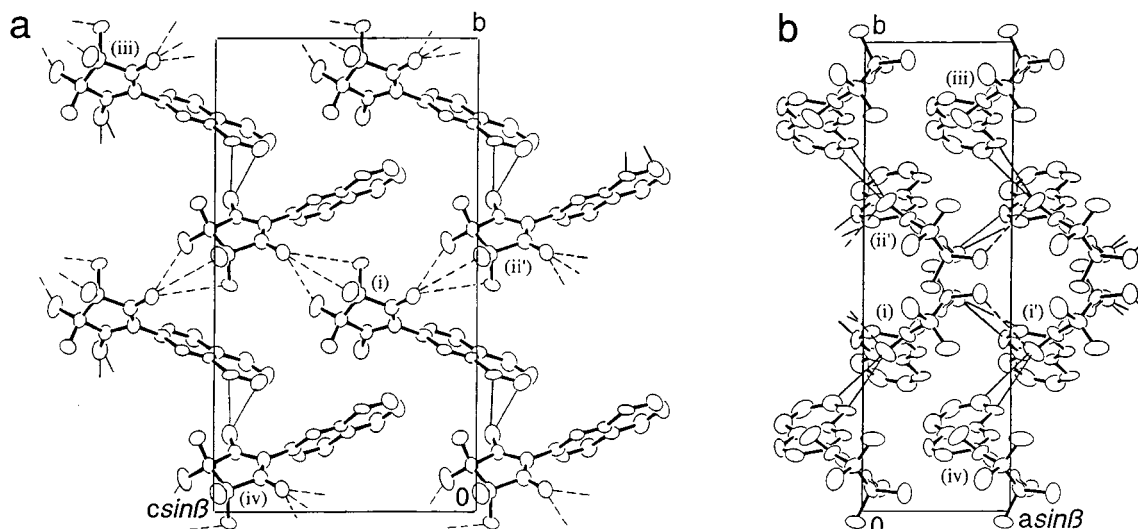
point of the b axis are oriented in an direction opposite to those in the other half. The lack of a screw axis does not give intermolecular contacts between the two adjacent quinolyl rings. Instead, there are contacts between the O atoms of the ONCNO group and the quinolyl rings, as shown by the solid lines in Fig. 5.

4-QNNN crystallizes in the triclinic system with space group $P\bar{1}$ and $Z = 2$. The crystal structure projected along the b and c axes is shown in Figs. 6a and 6b. The molecular arrangement in 4-QNNN is quite different from that of 1-NAPNN, in spite of the very similarly shaped molecules. As can be seen in Fig. 6b, the 4-QNNN molecules form a dimeric structure. Within the molecular dimer, there are intermolecular contacts between the N and O atoms of the NO groups and between the O atom of the NO group and the quinolyl ring. The interatomic distances are listed in Table 7. The interatomic contacts are doubled as a result of the inversion center between each dimer. The intermolecular arrangement in the dimer is depicted in Fig. 6c. The interatomic distance N1(i)–O1(ii′), 3.637(7) Å, indicates that one of the NO groups of the 4-QNNN molecule is quite close to the NO group of the other molecule in the dimer.

Each dimer is surrounded by eight neighboring dimers; two each are located along the a, b, and c axes and two along the [$\bar{1}$10] direction. Among them, there are intermolecular contacts between the neighboring molecules in the two dimers related by the translation symmetry along the [$\bar{1}$10] direction, as shown by the dotted lines in Figs. 6a and 6b. The relevant intermolecular interatomic distances

FIG. 4. Crystal structure of 2-QNNN: 3D network structure projected along (a) the *a* axis and (b) the *c* axis. Note that the molecules are oriented in the same direction along the *c* axis. Solid and dashed lines represent the intermolecular contacts relevant to magnetic interaction. For the symmetry operations, see Table 5.

are also listed in Table 7. These interatomic contacts are doubled because of the inversion symmetry at the center of the two molecules. The intermolecular arrangement between the neighboring molecules of adjacent dimers are shown in Fig. 6d. The quinolyl rings overlap in the so-called "ring-over-bond" fashion often observed for planar aromatic cyclic compounds. The interplanar distance 3.38(2) Å is comparable to that of polycyclic hydrocarbon radicals (35). Considerable molecular–orbital overlap is therefore expected between the neighboring quinolyl rings.

Magnetic Properties

The product of the paramagnetic susceptibility χ_p and temperature T of 1- and 2-NAPNN is plotted as a function of T in Fig. 7 (Note the logarithmic scale of T). In 1-NAPNN, the product $\chi_p T$, which is proportional to the

TABLE 5
Intermolecular Distances of 2-QNNN[a]

Intralayer contact	$r/\text{Å}$	Interlayer contact	$r/\text{Å}$
O1(i)–C13(ii′)	3.65(2)	O2(i′)–C2(iv)	3.08(1)
O1(i)–C14(ii′)	3.54(1)	O2(i′)–C3(iv)	3.42(2)
O1(i)–C16(ii′)	3.37(2)		
O1(i)–C7(i′)	3.43(1)		
O1(i)–C8(i′)	3.24(1)		
O2(i′)–C13(i)	3.51(2)		

[a] Symmetry operations: (i) x, y, z, (i′) $1 + x, y, z$, (ii′) $x, 1 - y, -1/2 + z$, (iii) $1/2 + x, 1/2 + y, z$, (iv) $1/2 + x, 1/2 - y, 1/2 + z$.
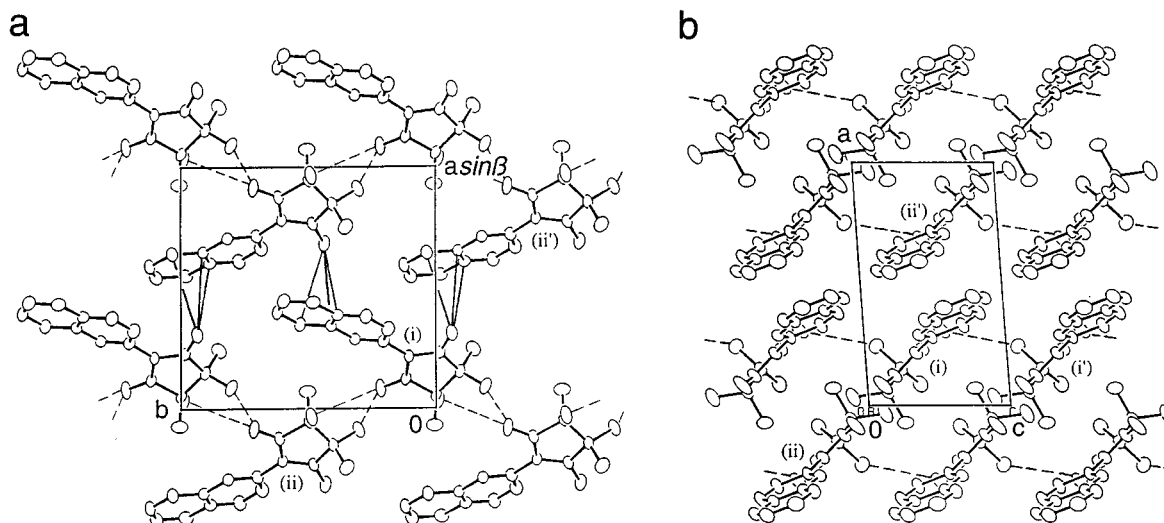
square of effective magnetic moment μ_{eff}^2, continues to increase with decreasing temperature down to the lowest temperature examined (1.8 K). On the other hand, in 2-NAPNN, $\chi_p T$ decreases slightly with decreasing temperature. These results suggest that the predominant intermolecular interaction is ferromagnetic in 1-NAPNN and antiferromagnetic in 2-NAPNN. The magnetization isotherms of 1- and 2-NAPNN measured at temperatures 1.8, 5, and 10 K are shown in Fig. 8 together with the theoretical curves for noninteracting paramagnets with $S = 1/2$ and 1 (Note that the scale of magnetization M for 2-NAPNN is offset for clarity). The slope of the magnetization isotherms of 1-NAPNN becomes steeper and closer to the $S = 1$ curve as the temperature decreases, providing further evidence for the presence of FM intermolecular interaction in this compound. In contrast, the magnetization isotherms of 2-NAPNN follow the $S = 1/2$ curve from 1.8 to 10 K, consistent with the fact that $\chi_p T$ is almost independent of temperature.

Figure 9a shows that temperature dependence of $\chi_p T$ for 2-, 3-, and 4-QNNN (26–28), while Fig. 9b shows the low-temperature behavior of 2- and 3-QNNN on the same scale as that for 1- and 2-NAPNN. The $\chi_p T$ values of 2- and 3-QNNN increase monotonically with decreasing temperature down to the lowest temperature examined (1.8 K), indicating FM intermolecular interactions in these two compounds. In contrast, for 4-QNNN, $\chi_p T$ decreases quite steeply with decreasing temperature, suggesting strong AFM intermolecular interaction. Figure 10 shows magnetization isotherms of 2- and 3-QNNN recorded at 1.8, 4, and 10 K together with the theoretical curves for non interacting

FIG. 5. Crystal structure of 3-QNNN: 3D network structure projected along (a) the *c* axis and (b) the *b* axis. Note that the molecules are oriented in the same direction along the b axis. Solid and dashed lines represent the intermolecular contacts relevant to magnetic interaction. For the symmetry operations, see Table 6.

paramagnets with $S = 1/2$ and 1. The magnetization isotherms of 3-QNNN rise more steeply at lower temperature, which is further evidence of the presence of FM intermolecular interaction. The magnetization isotherms of 2-QNNN almost follow the $S = 1/2$ curve, though the magnetization at 1.8 K deviates slightly upward from the $S = 1/2$ curve indicating weak but measurable FM intermolecular interaction. This result agrees with the weak temperature dependence of $\chi_p T$ observed for this compound.

Below, we describe quantitative analyses of the magnetic properties of 1- and 2-NAPNN and 2- and 3-QNNN in terms of combinations of FM interactions in the 2D layers with interlayer FM or AFM interaction on the basis of the isotropic Heisenberg model with the spin Hamiltonian $\mathcal{H} = -2J\sum\mathbf{S}_i\mathbf{S}_j$ and a mean molecular field approximation (36,37). Following the discussion of the crystal structures in the previous section, the 2D layers are approximated by ferromagnetically coupled square lattices of $S = 1/2$ spins, although the actual spin lattices would be more complic-

ated. Similar results are obtained using a triangular 2D FM spin lattice model. The magnetic properties of 4-QNNN are fitted to an alternating 1D AFM Heisenberg model based on the spin Hamiltonian $\mathcal{H} = -2J\sum(\mathbf{S}_{2i-1}\mathbf{S}_{2i} + \alpha\mathbf{S}_{2i}\mathbf{S}_{2i+1})$ (38).

The structural results for 1-NAPNN suggest that its magnetic behavior should be 3D but with intralayer exchange interactions different from those for interlayer. Thus, the intralayer FM interactions are described by the 2D Heisenberg model and interlayer couplings are modeled in the frame of the mean molecular field approximation. Assuming isotropic Heisenberg interactions, the temperature dependence of the magnetic susceptibility of a ferromagnetically coupled square lattice of $S = 1/2$ spins is described by the following high-temperature-series-expansions expression (36),

$$\chi_{2D}T = C[1 + 2x + 2x^2 + (4/3)x^3 + (13/12)x^4 + (71/60)x^5$$

$$+ (367/720)x^6 - (811/2520)x^7 + (8213/20160)x^8$$

$$+ (12103/11340)x^9 - (2514101/3628800)x^{10}],$$

[1]

with $x = J/(kT)$, where $C = Ng^2\mu_B^2/(4k)$ is the Curie constant for $S = 1/2$ spins, J is the exchange coupling constant, and k is the Boltzmann constant. The temperature dependence of total paramagnetic susceptibility χ_p is

$$\chi_p = \chi_{2D}[1 - 2zJ'\chi_{2D}/(Ng^2\mu_B^2)]^{-1}$$

[2]

TABLE 6
Intermolecular Distances of 3-QNNN[a]

Intralayer contact	$r/\text{Å}$	Interlayer contact	$r/\text{Å}$
O2(i)–C13(ii)	3.28(1)	O1(i)–C4(ii′)	3.696(9)
O2(i)–C15(ii)	3.44(2)	O1(i)–C5(ii′)	3.75(1)
O1(i)–C16(i′)	3.52(1)	O1(i)–C6(ii′)	3.720(9)

[a] symmetry operations: (i) x, y, z, (i′) $x, y, 1 + z$, (ii) $-x, 1 - /2 + y, -z$, (ii′) $1 - x, -1/2 + y, 1 - z$.
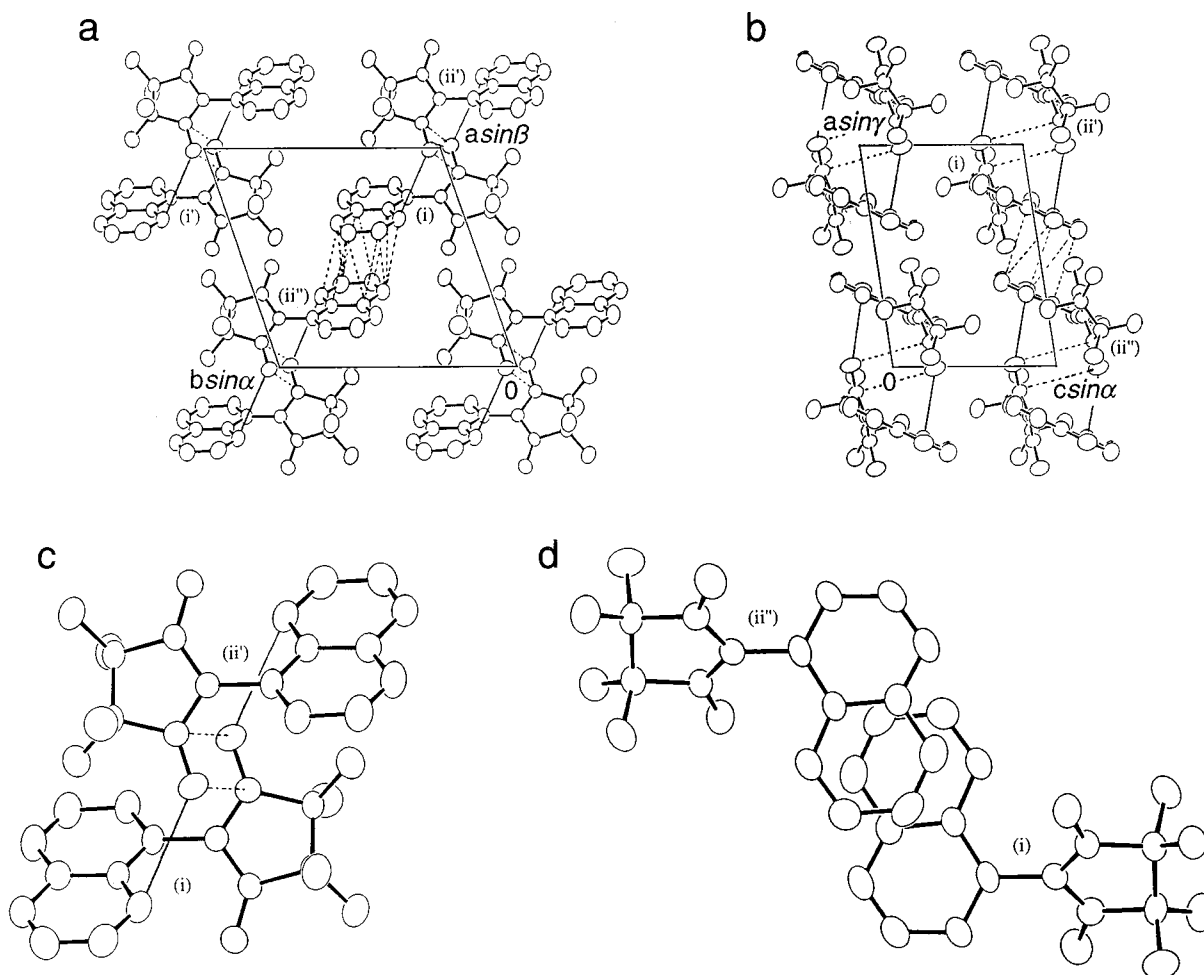
FIG. 6. Crystal structure of 4-QNNN projected along (a) the *c* axis and (b) the *b* axis. Dotted lines represent intermolecular contacts in the alternating molecular chain along the [$\bar{1}$10] direction. Intermolecular arrangements (c) between the molecules i and ii′ and (d) between the molecules i and ii″ in the crystal of 4-QNNN. For the symmetry operations, see Table 7.

where J' is the interlayer interaction and $z = 2$ is the number of adjacent layers (37). Fitting the $\chi_p T$ data to Eqs. [1] and [2] gives a good agreement as shown in the solid line in Fig. 7. The best fit values are $C = 0.387$ emu K mol^{-1}, $J/k = 0.09$ K and $J'/k = 0.03$ K. The Curie constant is close to that expected for a paramagnetic system with $g = 2.0067$, which is the average g factor for the nitronyl nitroxide radicals (23), and $S = 1/2$. The positive values of J/k and J'/k indicate that both intralayer and interlayer intermolecular interactions are ferromagnetic in 1-NAPNN. This result clearly suggests that the intermolecular contacts forming the 3D network shown in the previous section are relevant to the FM intermolecular interaction.

It is shown that two kinds of intermolecular contacts, the contacts between the O atoms of the NO groups and the H atoms of the methyl groups and those between the ONCNO groups and naphthyl rings, form the 3D network of 1-NAPNN. The contacts between the NO and methyl

groups are theoretically predicted (39) to be responsible for FM intermolecular interaction through the hydrogen bonds NO $\cdots$ HC. The contacts between the ONCNO group and

TABLE 7
Intermolecular Distances of 4-QNNN[a]

Intradimer contact	$r/Å$	Interdimer contact	$r/Å$
N1(i)–O1(ii′)	3.637(7)	O2(i)–C10(ii″)	3.470(8)
O1(i)–C7(ii′)	3.417(9)	C5(i)–C8(ii″)	3.59(1)
		C5(i)–C9(ii″)	3.42(1)
		C6(i)–C9(ii″)	3.54(1)
		C6(i)–C10(ii″)	3.65(1)
		C7(i)–C10(ii″)	3.56(1)
		C8(i)–C10(ii″)	3.54(1)
		C9(i)–C10(ii″)	3.64(1)

[a] Symmetry operations: (i) x, y, z, (ii′) $2 - x$, $- y$, $2 - z$, (ii″) $1 - x$, $1 - y$, $2 - z$.
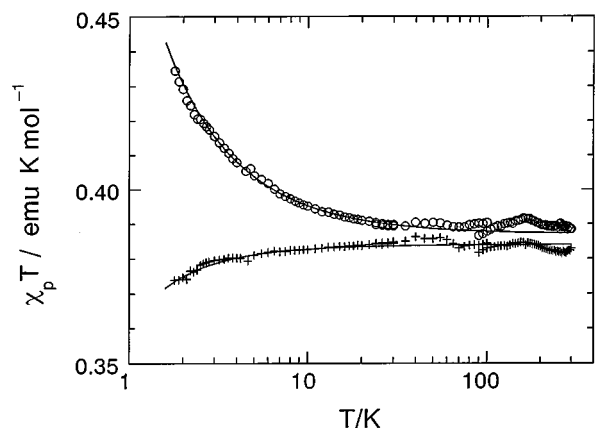
FIG. 7. Temperature dependence of $\chi_p T$ of 1-NAPNN (circles) and 2-NAPNN (crosses). Solid lines represent $\chi_p T$ calculated in terms of anisotropic 3D magnetic interaction models (see text). Note the logarithmic scale of T.

the naphthyl ring may result in SOMO–NHOMO and/or SOMO–NLUMO (next-lowest unoccupied molecular orbital) overlaps which favor FM intermolecular interaction in odd alternant hydrocarbons like nitronyl nitroxide (30), because the SOMO of nitronyl nitroxide substituted with aromatic rings is predominantly localized on the NO groups while NHOMO and NLUMO are extended to the aromatic rings (40). The magnetic exchange paths in 1-NAPNN therefore form a 3D FM network through the two kinds of intermolecular contacts mentioned above.

By using the coupling constants obtained, we have estimated the FM phase transition temperature T_c in terms of the Langevin–Weiss model (41). In the model, T_c is related
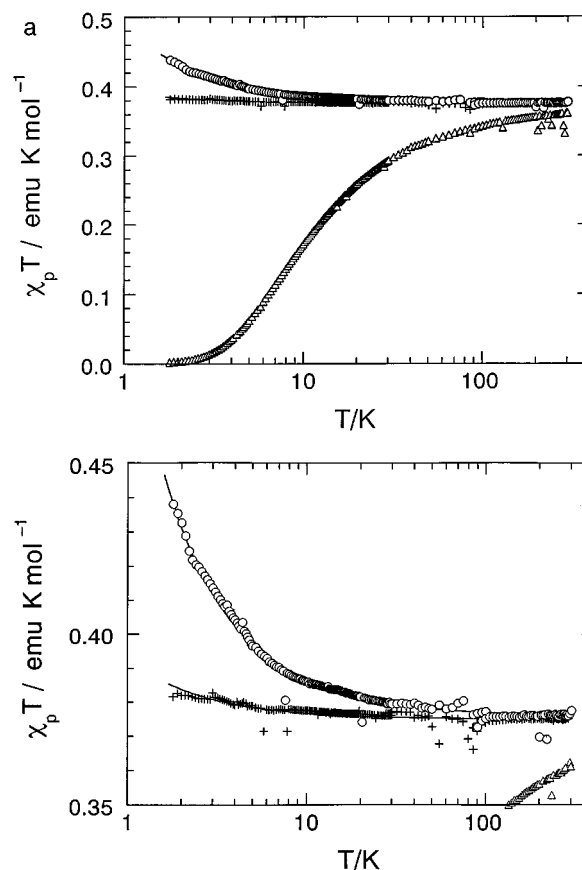

FIG. 9. (a) Temperature dependence of $\chi_p T$ of 2-QNNN (crosses), 3-QNNN (circles), and 4-QNNN (triangles). (b) Low-temperature behavior of 2- and 3-QNNN on the same scale of M as Fig. 7. Solid lines represent $\chi_p T$ calculated in terms of anisotropic 3D magnetic interaction models (see text). Note the logarithmic scale of T.
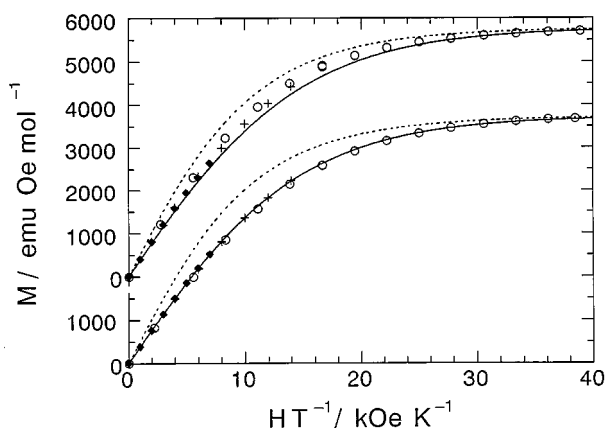
to the intermolecular coupling constants J_{ab} by

$$kT_c = 2S(S + 1)\sum J_{ab}/3. \qquad [3]$$

In our analysis, a spin site with $S = 1/2$ is coupled to four $S = 1/2$ sites with $J/k = 0.09$ K and two $S = 1/2$ sites with $J'/k = 0.03$ K. By using Eq. [3], T_c is estimated to be 0.21 K. We have found that 1-NAPNN exhibits a magnetic phase transition at 0.10 K by using the muon spin rotation/relaxation (μSR) techniques (31). Since a large relaxation component is observed in the μSR data, there seem to be strong fluctuations of the spin magnetic moments, which may reduce T_c.

The structural results for 2-NAPNN suggest that its magnetic behavior could be modeled by a similar approach to the one applied to 1-NAPNN. Equations [1] and [2] give a good fit to the $\chi_p T$ data, as shown by the solid line in Fig. 7. The best fit values are $C = 0.384$ emu K mol^{-1}, $J/k = 0.14$ K, and $J'/k = -0.31$ K, the negative value of J'/k suggesting AFM interlayer interaction. The fact

FIG. 8. Magnetization isotherms of 1-NAPNN (upper) and 2-NAPNN (lower) measured at 1.8 K (circles), 5 K (crosses), and 10 K (diamonds). Note that the scale of magnetization M of 2-NAPNN is offset for clarity. Solid and broken lines represent the isotherms calculated with the Brillouin function for $S = 1/2$ and 1, respectively.
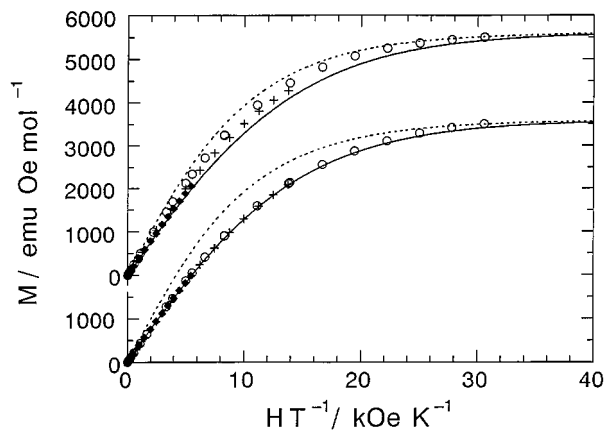
FIG. 10. Magnetization isotherms of 2-QNNN (lower) and 3-QNNN (upper) measured at 1.8 K (circles), 4 K (crosses), and 10 K (diamonds). Note that the scale of M of 2-QNNN is offset for clarity. Solid and broken lines represent the isotherms calculated with the Brillouin function for $S = 1/2$ and 1, respectively.

that the absolute value of J'/k is twice as large as J/k indicates that the predominant intermolecular interaction is the AFM interaction. The positive value of J/k and hence the intralayer FM interaction indicates that the intermolecular contacts between the O atoms of the ONCNO group and the methyl groups froming the 2D layers of 2-NAPNN can be correlate with the FM intermolecular interaction.

In contrast, the contacts between the neighboring naphthyl rings that lie face to face across the interface between the 2D molecular layers should be correlated with the AFM intermolecular interaction. Since the contacts between the naphthyl rings increase the SOMO–SOMO overlap, an AFM interaction is favored (30). The overlap, however, would be reduced because the planes of the naphthyl rings make a dihedral angle 46°. There is another contact between the OCNCO and naphthyl groups. As shown for 1-NAPNN, this contact may favor FM intermolecular interaction, introducing competetion between FM and AFM interactions in adjacent 2D molecular layers. The small overlap between the neighboring naphthyl rings and the competition of FM and AFM interactions may result in the weak interlayer AFM interaction actually observed.

The structural results for 2-QNNN again suggest an approach to the magnetic properties similar to that applied to the two isomers of NAPNN. In fact, Eqs. [1] and [2] give a good fit to the $\chi_p T$ data, as shown by the solid line in Fig. 9b. The best fit values are $C = 0.375$ emu K mol^{-1}, $J/k = 0.018$ K, and $J'/k = 0.010$ K, suggesting that both intralayer and interlayer intermolecular interactions are ferromagnetic in 2-QNNN. Since, as discussed for 1-NAPNN, all the contacts forming the 3D network contribute to FM interaction, the magnetic exchange paths through the intermolecular contacts in 2-QNNN should result in a 3D FM

network as actually observed. It is worth noting that, in contrast to 2-NAPNN, there is no overlap between the quinolyl rings to favor AFM interaction while the molecular arrangements in the 2D layers are both herringbone-like and similar to each other. On the basis of the coupling constants and Eq. [3], the FM transition temperature is estimated to be 0.05 K.

Although the temperature dependence of $\chi_p T$ of 3-QNNN was analyzed previously using a simple molecular mean field model, which yields a Weiss constant $\theta = 0.28$ K (26), the data are reexamined here because the fitting at temperatures lower than 3 K gave no satisfactory agreement with the simple mean field model. The structural results for 3-QNNN suggest 3D models similar to those applied to 2-QNNN and hence we would not expect the simple mean field model to provide an adequate description. Fitting the $\chi_p T$ data to Eqs. [1] and [2] gives a better agreement than fitting to the simple mean field model, as shown by the solid line in Fig. 9b. The best fit values are $C = 0.376$ emu K mol^{-1}, $J/k = 0.12$ K, and $J'/k = 0.03$ K. The exchange coupling constant $J/k = 0.12$ K in the 2D layers is consistent with the Weiss constant $\theta = 0.28$ K reported previously, because a Weiss constant is related to a coupling constant by the relation $\theta = 2zJS(S + 1)/(3k)$. Since $z = 4$ for a square lattice, $\theta = 2J/k$. Our result $\theta = 2.3J/k$ is close to this relation. The positive values of J/k and J'/k suggest that both intralayer and interlayer interactions are ferromagnetic in 3-QNNN, which is consistent with the 3D FM exchange paths predicted from the intermolecular contacts referring to the discussions for 1- and 2-NAPNN and 2-QNNN. Using the fitted values of the exchange constants and Eq. [3], T_c is estimated to be 0.27 K. This is close to the phase transition temperature 0.23 K actually observed for 3-QNNN by μSR and a.c. susceptibility measurements (19). Clear observation of μSR oscillations below T_c suggests a well developed magnetic order, which does not reduce T_c very much (14).

The structural features of 4-QNNN suggest an alternating 1D chain model, quite different from the model applied to the other radicals we have discussed. The contacts between the NO groups, on which the SOMO is localized, would yield large SOMO–SOMO overlap, thus favoring AFM intermolecular interaction in the molecular dimers. The dimers form a 1D array along the $[\bar{1}10]$ direction through the face-to-face overlap between the quinolyl rings, also favoring AFM interaction. By assuming isotropic Heisenberg interactions, the temperature dependence of the magnetic susceptibility of an alternating array of antiferromagnetically coupled $S = 1/2$ spins is described by the following series-expansions with the alternation parameter $\alpha = J'/J$,

$$\chi_p T = C(1 + 0.5998x + 1.20376x^2)/$$
$$(1 + 1.9862x + 0.68854x^2 + 6.0626x^3) \quad [4]$$

for $\alpha = 1$,

$$\chi_p T = C[1 + (-0.5478 + 1.05548\alpha)x$$
$$+ (0.0681 - 0.50672\alpha + 1.96452\alpha^2 - 4.7908\alpha^3$$
$$+ 3.49028\alpha^4)x^2]/[1 + (0.070509 + 1.3042\alpha)x$$
$$+ (-0.0035767 - 0.40837\alpha$$
$$+ 3.4862\alpha^2 - 0.73888\alpha^3)x^2$$
$$+ (0.36184 - 0.065528\alpha + 6.65875\alpha^2$$
$$- 20.945\alpha^3 + 15.425\alpha^4)x^3] \qquad [5]$$

for $0.4 < \alpha < 1$, and

$$\chi_p T = C[1 + (-0.50348 + 0.91008\alpha)x$$
$$+ (0.076444 - 0.53228\alpha + 2.036\alpha^2 - 5.2668\alpha^3$$
$$+ 4.0324\alpha^4)x^2]/[1 + (0.10772 + 1.4192\alpha)x$$
$$+ (-0.0028521 - 0.4236\alpha + 2.1953\alpha^2$$
$$- 0.82412\alpha^3)x^2 + (0.37754 - 0.067022\alpha + 6.9805\alpha^2$$
$$- 21.678\alpha^3 + 15.838\alpha^4)x^3] \qquad [6]$$

for $0 < \alpha \le 0.4$, where $x = |J|/(kT) \le 2$ and $J < 0$ (38,42). For the reduced temperatures $T_r = x^{-1}$ less than 0.5, only extrapolated χ_p values are available for several values of α (38). For $\alpha = 0$, χ_p is calculated by using the analytical formula

$$\chi_p T = 4C[3 + \exp(2y)]^{-1} \qquad [7]$$

where $y = J/(kT)$ (43). The temperature dependence of χ_p of 4-QNNN is shown in Fig. 11 together with that calculated for $\alpha = 0, 0.4, 0.6$, and 1 by using Eqs. [4] and [7] and the extrapolated curves reported (38). As clearly seen in Fig. 11, the experimental data lie between the curves calculated and extrapolated with $\alpha = 0.4$ and 0.6. The best fit values obtained with Eq. [5] for the data at temperatures higher than 3.9 K $(=|J|/2k)$ are $C = 0.376$ emu K mol^{-1}, $J/k = -7.8$ K, and $\alpha = 0.53$ (i.e., $J'/k = -4.1$ K). The theoretical curve calculated from these parameters is shown by the solid line in Fig. 11. The slight upward deviation at temperatures lower than 2.5 K is probably due to a small amount (less than 0.5%) of uncoupled spins.

Magneto-Structural Correlation

The similar 2D herringbone-like packing of molecules formed in 2-NAPNN, 2-QNNN, and 3-QNNN follows from the similar shape of these three nitronyl nitroxide molecules, in contrast to the other isomers 1-NAPNN and
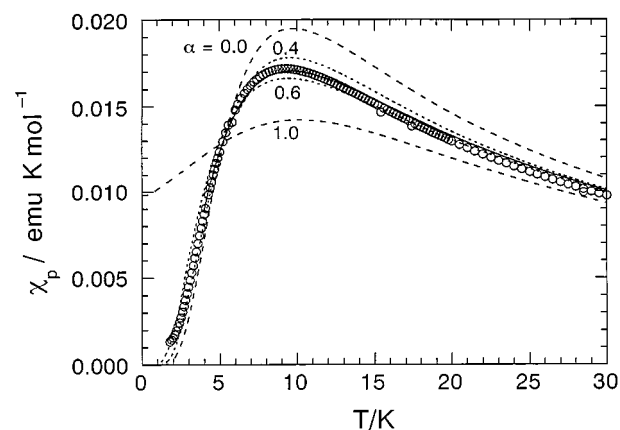

FIG. 11. Temperature dependence of χ_p of 4-QNNN shown by circles. Solid line represents χ_p calculated in terms of the alternating one-dimensional antiferromagnetic Heisenberg model with $J/k = -7.8$ K and alternation parameters $\alpha = 0.53$ (see text). Dotted lines show χ_p calculated and extrapolated for $\alpha = 0.4$ and 0.6. Broken lines demonstrate χ_p for the singlet–triplet model ($\alpha = 0$) and the uniform antiferromagnetic Heisenberg model ($\alpha = 1$) with the same J/k value.

4-QNNN, which crystallize in rather different molecular arrangements. From our analyses of the temperature dependence of the paramagnetic susceptibilities, we find that the magnetic behavior of the compounds with 2D molecular arrangements are convincingly described by a 2D spin lattice with FM intermolecular interactions. We therefore conclude that the FM intermolecular interactions in 2-NAPNN, 2-QNNN, and 3-QNNN result from the interatomic contacts that form the 2D molecular layers.

Two kinds of interatomic contact are responsible for the 2D FM intermolecular interactions in 2-NAPNN, 2-QNNN, and 3-QNNN: one is the contact between the O atom of the ONCNO group and the methyl groups, and the other is between the O atom of the ONCNO group and the C (or H) atoms of the quinolyl ring. As summarized in Table 8, the former are observed in all three crystals, while the latter are observed only in 2-QNNN, reflecting the close similarity between the molecular arrangements in the 2D layers of 2-NAPNN and 3-QNNN. Therefore, the contacts between the O atom and methyl groups are definitely related to the FM intermolecular interaction in nitronyl nitroxide radical crystals.

Our analysis of the temperature dependent susceptibility also suggests that the interlayer contacts observed in 2- and 3-QNNN are likewise responsible for the FM interactions. Those relevant to the FM interaction are between the O atom of the ONCNO group and the C atoms of the quinolyl ring as listed in Table 8. This kind of contact is also observed in the 2D layer of 2-QNNN, when it gives rise to intralayer FM intermolecular interaction as mentioned above. Therefore, the contacts between the O atom of the ONCNO group and the C atoms of the quinolyl ring also

TABLE 8
Intermolecular Contacts Relevant to Magnetic Interactions in the Isomers of NAPNN and QNNN

Intermolecular contacts	Relevant interactions	1-NAPNN	2-NAPNN	2-QNNN	3-QNNN	4-QNNN[a]
*Intra*layer						
ONCNO ⋯ H₃C–	ferromagnetic	yes	yes	yes	yes	no
ONCNO ⋯ ring	ferromagnetic	yes	no	yes	no	no
*Inter*layer						
ONCNO ⋯ H₃C–	ferromagnetic	yes	no	no	no	no
ONCNO ⋯ ring	ferromagnetic	yes	yes	yes	yes	no
ring ⋯ ring	antiferromagnetic	no	yes	no	no	yes
ONCNO ⋯ ONCNO	antiferromagnetic	no	no	no	no	yes
Overall magnetic beahvior		ferromag.	antiferro.	ferromag.	ferromag.	antiferro.

[a] No layer structure is observed.

give rise to the FM interactions as theoretically predicted (30). As shown in Table 8, the same two kinds of interatomic contacts are also formed in 1-NAPNN, which exhibits 3D FM interaction, although the molecular packing arrangement is quite different from those in 2-NAPNN, 2-QNNN, and 3-QNNN, discussed above. Therefore, we must conclude that intermolecular contacts between the ONCNO group on one molecule and the methyl groups of nitronyl nitroxide or polycyclic ring moieties of neighboring molecules give rise to FM interactions in several different ways.

Because the details of the molecular packing are so crucial to the bulk magnetic behavior, it is worth analyzing the intermolecular contacts more closely. Figure 12a presents a schematic view of the intermolecular contacts between the ONCNO group of a nitronyl nitroxide molecule and the methyl groups of a neighboring molecule as observed in the crystals of 2-NAPNN, 2-QNNN, and 3-QNNN. The distances between the O atom and the four methyl carbon atoms are listed in Table 9. Although the ambiguity in determining the positions of the H atoms of the methyl groups hinders more elaborate discussion, the fact that at least one O–C distance in each compound is shorter than the sum (3.4 Å) of van der Waals radii of O atom and methyl group clearly suggests weak hydrogen bonding between the O and the H atoms of the methyl group. The reason for these contacts is H ⋯ O attraction because of the large negative charges on the O atoms of the ONCNO group (40). Steric repulsion between the four methyl groups elongates several of the O ⋯ H₃C contacts beyond 3.8 Å, while one of the four O–C distances is shorter than the sum of van der Waals radii. Since the N–O bonds are nearly perpendicular to the long axes of the molecules, it is the conjunction of the O atom with the four methyl groups that determines the herringbone-like molecular packing.

Figure 12b gives a schematic view of the intermolecular contacts between the N atom of a quinolyl ring and the methyl groups of a neighboring nitronyl nitroxide molecule in the 4-QNNN crystal. The N–C distances between the

quinolyl N and the four methyl C atoms are 3.783(9) Å; N3–C15, 3.866(9) Å; N3–C14, 3.935(9) Å; N3–C16 and 5.078(9) Å; N3–C13. Although there are no interatomic distances shorter than the sum (3.5 Å) of the van der Waals radii of N and the methyl group in 4-QNNN, the N atom is quite evidently surrounded by four methyl groups of a neighboring molecule at a position related by the translation symmetry operation along the *b* axis. Again, the most probable explanation is H ⋯ N attraction.

No coordination of the quinolyl N atom to the methyl groups of a neighboring molecule is observed in either of the other QNNN isomers; indeed, such coordination would be difficult, especially for 2-QNNN, because of steric repulsion between the NO group of one molecule and a part of methyl groups of the other. On the contrary, the contact between the O atom and the four methyl groups seen in 2- and 3-QNNN is prevented in 4-QNNN by steric hindrance from the second ring of the quinolyl group and part of the methyl groups. It is the characteristic molecular shape of 4-QNNN and the existence of a N atom at the opposite side of the nitronyl nitroxide moiety that bring about the coordination of the quinolyl N atom to the four methyl groups unique among this series.

The molecular packing arrangement in 1-NAPNN is quite different from that of 4-QNNN despite their nearly identical molecular shapes. The substitution of N on the quinolyl ring of 4-QNNN by CH ruptures the atomic coordination observed in 4-QNNN, since there is no longer an electronegative atom close to the nitronyl nitroxide moiety. Furthermore, in 1-NAPNN, the approach of the O atom to the four methyl groups observed in 2-NAPNN and 2- and 3-QNNN is inhibited by steric hindrance between the second naphthyl ring and part of the methyl groups. These structural restrictions, which differ from those in the other nitronyl nitroxide crystals, result in the unique molecular packing arrangement in 1-NAPNN. In the 1-NAPNN crystal, one of the four methyl groups of the nitronyl nitroxide moiety with the symmetry operation (i) is coordinated by
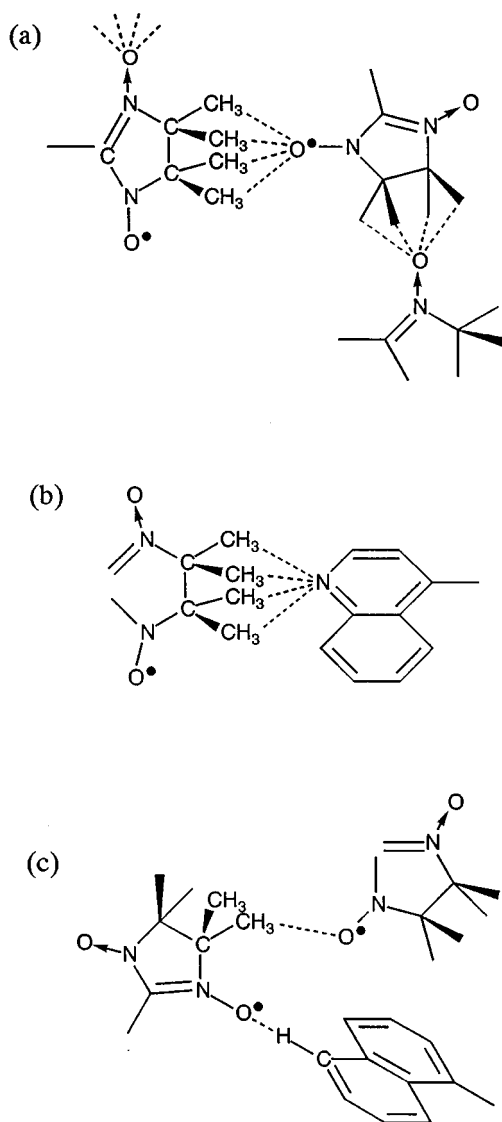
FIG. 12. (a) A schematic view of NO ⋯ H$_3$C contacts in 2-NAPNN, 2-QNNN, and 3-QNNN. (b) A schematic view of =N̄ ⋯ H$_3$C contacts in 4-QNNN. (c) A schematic view of NO ⋯ H$_3$C and NO ⋯ HC= contacts in 1-NAPNN.

also dominated by hydrogen bonds as observed in the other radical crystals.

CONCLUSIONS

We have shown that in the isomeric series of naphthyl nitronyl nitroxide (NAPNN) and quinolyl nitronyl nitroxide (QNNN) the intermolecular magnetic interactions are rich in variety, ranging from ferromagnetic to antiferromagnetic. The magnetic interactions are found to be strongly related to the packing of the molecular radicals in the crystals. In particular, 2-NAPNN and 2- and 3-QNNN, having quite close molecular shapes, crystallize in a characteristic herringbone-like packing arrangement, forming layers, within which a FM interaction is established. On the other hand, 1-NAPNN exhibits FM intermolecular interaction through molecular arrangements quite different from those of 2-NAPNN and 2- and 3-QNNN. In the crystals exhibiting FM intermolecular interactions, close contacts are observed between the O atoms of the ONCNO groups and the methyl groups as well as between the O atoms and the naphthyl and quinolyl rings. We conclude therefore that it is these contacts that are responsible for the FM interaction in this class of crystalline radicals, independent of their individual molecular packing arrangements.

An important feature of the molecular packing is the hydrogen bonds between the O atoms of the NO groups and the H atoms of the methyl and naphthyl groups, and (in 4-QNNN) between the quinolyl N atom and H atoms of the methyl groups. The other major influence on the molecular packing is, of course, the shape of the radicals through steric hindrance between adjacent molecules.

The packing of the molecules in the crystals of 2-NAPNN and 3-QNNN presents some very similar features. However, eliminating the electronegative N from 3-QNNN induces a change of crystal symmetry and hence a partial difference in the overall molecular arrangement. Thus, in the crystal of 2-NAPNN the radical molecules in the 2D layer are oriented inversely to those in adjacent layers, while the 3-QNNN molecules are oriented in the same direction in all the layers. This small alteration in the molecular packing

the O atom of the ONCNO group of a neighboring molecule at the position with the symmetry operation (ii′). In addition, the O atom of the ONCNO group of the molecule (i) coordinates to a naphthyl H atom on the other neighboring molecule at the position with the symmetry operation (ii), as shown in Fig. 12c. The relevant interatomic distances are 3.41(2) Å for O1(ii′)–C14(i) (NO ⋯ H$_3$C contact) and 2.61 Å for O2(i)–H–C7(ii) (NO ⋯ HC = contact). Since both the O–C and O–H interatomic distances are almost identical to the sum of the van der Waals radii for O–CH$_3$ (3.4 Å) and O–H (2.6 Å), the molecular packing in 1-NAPNN is

TABLE 9
Intermolecular Distances of 2-NAPNN, 2-QNNN, and 3-QNNN

Compound	Contact	r/Å	Contact	r/Å
2-NAPNN	O1–C14	3.256(8)	O1–C15	3.866(8)
	O1–C16	3.514(8)	O1–C17	3.838(8)
2-QNNN	O1–C13	3.65(2)	O1–C14	3.54(2)
	O1–C15	4.57(2)	O1–C16	3.37(2)
3-QNNN	O2–C13	3.28(1)	O2–C14	3.84(1)
	O2–C15	3.44(1)	O2–C16	3.84(1)

results in a drastic change in magnetic behavior of the crystal as a whole: that is to say, it changes from ferromagnetic in 3-QNNN to antiferromagnetic in 2-NAPNN.

In conclusion, to control the packing arrangements of the molecules and hence the magnetic interaction in organic radical crystals more precisely, it is essential to invoke specific intermolecular interactions such as hydrogen bonds and electrostatic attractive forces as well as the shape of the radical molecules.

ACKNOWLEDGMENTS

REFERENCES

1. See for example, Proceedings of International Conference on Molecule-Based Magnets, *Mol. Cryst. Liq. Cryst.* **232–233** (1993); **271–274** (1995); **305–306** (1997).

2. M. Tamura, Y. Nakazawa, D. Shiomi, K. Nozawa, Y. Hosokoshi, M. Ishikawa, M. Takahashi and M. Kinoshita, *Chem. Phys. Lett.* **186,** 401 (1991).

3. T. Sugawara, M. M. Matsushita, A. Izuoka, N. Wada, N. Takeda, and M. Ishikawa, *J. Chem. Soc., Chem. Commun.* 1723 (1994).

4. J. Cirujeda, M. Mas, E. Molins, F. L. de Panthou, J. Laugier, J. G. Park, C. Paulsen, P. Rey, C. Rovira, and J. Veciana, *J. Chem. Soc., Chem. Commun.* 709 (1995).

5. A. Caneschi, F. Ferraro, D. Gatteschi, A. le Lirzin, M. A. Novak, E. Rentschler, and R. Sessoli, *Adv. Mater.* **7,** 476 (1995).

6. R. Chiarelli, M. A. Novak, A. Rassat, and J. L. Tholence, *Nature* (*London*) **363,** 147 (1993).

7. T. Nogami, K. Tomioka, T. Ishida, H. Yoshikawa, M. Yasui, F. Iwasaki, H. Iwamura, N. Takeda, and M. Ishikawa, *Chem. Lett.* 29 (1994).

8. T. Ishida, H. Tsuboi, T. Nogami, H. Yoshikawa, M. Yasui, F. Iwasaki, H. Iwamura, N. Takeda, and M. Ishikawa, *Chem. Lett.* 919 (1994).

9. T. Nogami, T. Ishida, H. Tsuboi, H. Yoshikawa, H. Yamamoto, M. Yasui, F. Iwasaki, H. Iwamura, N. Takeda, and M. Ishikawa, *Chem. Lett.* 635 (1995).

10. K. Mukai, K. Konishi, K. Nedachi, and K. Takeda, *J. Magn. Magn. Mater.* **140–144,** 1449 (1995).

11. K. Takeda, T. Hamano, T. Kawae, M. Hidaka, M. Takahashi, S. Kawasaki, and K. Mukai, *J. Phys. Soc. Japan* **64,** 2343 (1995).

12. U. Welp, S. Fleshler, W. K. Kwok, G. W. Crabtree, K. D. Carlson, H. H. Wang, U. Geiser, J. M. Willams, and V. M. Hitsman, *Phys. Rev. Lett.* **69,** 840 (1992).

13. T. Sugimoto, M. Tsujii, H. Matsuura, and N. Hosoito, *Chem. Phys. Lett.* **235**, 183 (1995).

14. F. L. Pratt, R. Valladares, J. Caulfield, I. Deckers, J. Singleton, A. J. Fisher, W. Hayes, M. Kurmoo, P. Day, and T. Sugano, *Synth. Metals* **61,** 171 (1993).

15. S. Tomiyoshi, T. Yano, N. Azuma, M. Shoga, K. Yamada, and J. Yamauchi, *Phys. Rev. B* **49,** 16,031 (1994).

16. Y. Pei, O. Kahn, M. A. Aebersold, L. Ouahab, F. Le Berre, L. Pardi, and J. L. Tholence, *Adv. Mater.* **6,** 681 (1994).

17. R. K. Kremer, B. Kanellakopulos, P. Bele, H. Brunner, and F. A. Neugebauer, *Chem. Phys. Lett.* **230,** 255 (1994).

18. T. C. Kobayashi, M. Takiguchi, C. U. Hong, K. Amaya, A. Kajiwara, A. Harada, and M. Kamachi, *J. Magn. Magn. Mater.* **140–144,** 1447 (1995).

19. T. Sugano, F. L. Pratt, M. Kurmoo, N. Takeda, M. Ishikawa, S. J. Blundell, P. A. Pattenden, R. M. Valladares, W. Hayes, and P. Day, *Synth. Metals* **71,** 1827 (1995).

20. T. Sugano, M. Kurmoo, P. Day, F. L. Pratt, S. J. Blundell, W. Hayes, M. Ishikawa, M. Kinoshita, and Y. Ohashi, *Mol. Cryst. Liq. Cryst.* **271,** 107 (1995).

21. T. Kobayashi, M. Takiguchi, K. Amaya, H. Sugimoto, A. Kajiwara, A. Harada, and M. Kamachi, *J. Phys. Soc. Japan* **62,** 3239 (1993).

22. G. Choutou and C. Veyret-Jeandey, *J. Phys.* (*Paris*) **42,** 1441 (1981).

23. E. F. Ullman, J. H. Osiecki, D. G. B. Boocock, and R. Darcy, *J. Am. Chem. Soc.* **94,** 7049 (1972).

24. T. Sugano, T. Goto, and M. Kinoshita, *Solid State Commun.* **80,** 1021 (1991).

25. T. Sugano, T. Fukasawa, and M. Kinoshita, *Synth. Metals* **41–43,** 3281 (1991).

26. T. Sugano, M. Tamura, M. Kinoshita, Y. Sakai, and Y. Ohashi, *Chem. Phys. Lett.* **200**, 235 (1992).

27. T. Sugano, M. Tamura and M. Kinoshita, *Synth. Metals* **55–57**, 3305 (1993).

28. T. Sugano, M. Tamura, T. Goto, R. Kato, M. Kinoshita, Y. Sakai, Y. Ohashi, M. Kurmoo, and P. Day, *Mol. Cryst. Liq. Cryst.* **232,** 61 (1993).

29. K. Awaga and Y. Maruyama, *J. Chem. Phys.* **91,** 2743 (1989).

30. K. Awaga, T. Sugano, and M. Kinoshita, *Chem. Phys. Lett.* **141,** 540 (1987).

31. S. J. Blundell, T. Sugano, P. A. Pattenden, F. L. Pratt, R. M. Valladares, K. H. Chow, H. Uekusa, Y. Ohashi, and W. Hayes, *J. Phys.* **8,** L1 (1996).

32. M. Lamchen and T. W. Mittag, *J. Chem. Soc. C* 2300 (1966).

33. C. K. Johnson, "ORTEPII," ORNL Report 5138, Oak Ridge National Laboratory, Oak Ridge, TN, vol. 22, p. 833, 1976.

34. L. Pauling, "The Nature of the Chemical Bond," 3rd ed., Cornell University Press, Ithaca, NY, 1960.

35. For example; J.-J. André, A. Bieber, and F. Gautier, *Ann. Phys.* **1**, 145 (1976).

36. G. A. Baker, Jr., H. E. Gilbert, J. Eve, and G. S. Rushbrooke, *Phys. Lett. A* **25,** 207 (1967); *Phys. Rev.* **164,** 207 (1967).

37. J. N. McElearney, D. B. Losee, S. Merchant, and R. L. Carlin, *Phys. Rev. B* **7,** 3314 (1973).

38. J. C. Bonner, H. W. J. Blöte, J. W. Bray, and I. S. Jacobs, *J. Appl. Phys.* **50,** 1810 (1979).

39. A. Oda, T. Kawakami, S. Takeda, W. Mori, M. M. Matsushita, A. Izuoka, T. Sugawara, and K. Yamaguchi, *Mol. Cryst. Liq. Cryst.* **306,** 151 (1997).

40. K. Awaga, T. Inabe, U. Nagashima, and Y. Maruyama, *J. Chem. Soc., Chem. Commun.* 1617 (1989); 520 (1990).

41. M. Okumura, K. Yamaguchi, M. Nakano, and W. Mori, *Chem. Phys. Lett.* **207,** 1 (1993).

42. W. E. Hatfield, *J. Appl. Phys.* **52,** 1985 (1981).

43. B. Bleaney and K. D. Bowers, *Proc. R. Soc. London A* **214,** 451 (1952).